Evidence for Shock Acceleration and Intergalactic Magnetic Fields in a Large-Scale Filament of Galaxies ZwCl 2341.1+0000

Joydeep Bagchi [a,1,3] Torsten A. Enßlin [b,1]
Francesco Miniati [b,1] Stalin C.S. [c,1] M. Singh [c,1]
Somak Raychaudhury [d,1] Humeshkar N.B. [e,1,2]

[a] *Inter-University Centre for Astronomy and Astrophysics (IUCAA), Post Bag 4, Ganeshkhind, Pune 411007, India*

[b] *Max-Planck-Institut für Astrophysik, Karl-Schwarzschild-Str. 1, 85740 Garching, Germany*

[c] *State Observatory, Manora Peak, Naini Tal 263129, India*

[d] *School of Physics & Astronomy, University of Birmingham, Edgbaston, Birmingham B15 2TT, UK*

[e] *Dept. of Physics, Loyola College, University of Madras, Chennai 600034, India*

Abstract

We report the discovery of large-scale diffuse radio emission from what appears to be a large-scale filamentary network of galaxies in the region of cluster ZwCl 2341.1+0000, and stretching over an area of at least $6\,h_{50}^{-1}$ Mpc in diameter. Multicolour CCD observations yield photometric redshifts indicating that a significant fraction of the optical galaxies in this region is at a redshift of $z=0.3$. This is supported by spectroscopic measurements of 4 galaxies in the SDSS survey at a mean $z=0.27$. We present VLA images at λ =20 cm (NVSS) and 90 cm, showing the detailed radio structure of the filaments. Comparison with the high resolution FIRST radio survey shows that the diffuse emission is not due to known individual point sources. The diffuse radio-emission has a spectral index $\alpha \lesssim -0.5$, and is most likely synchrotron emission from relativistic charged particles in an inter-galactic magnetic field. Furthermore, this optical/radio structure is detected in X-rays by the ROSAT all-sky survey. It has a 0.1–2.4 keV luminosity of about 10^{44} erg s^{-1} and shows an extended highly non-relaxed morphology. These observations suggest that ZwCl 2341.1+0000 is possibly a proto-cluster of galaxies in which we are witnessing the process of structure formation. We show that the energetics of accretion shocks generated in forming large-scale structures are sufficient to produce enough high energy cosmic-ray (CR) electrons required to explain the observed radio emission, provided a magnetic field of strength $B \gtrsim 0.3\mu$G is present there. The latter is only a lower limit and the actual magnetic field is likely to be higher depending on the morphology of the emitting region. Finally, we show results from a numerical

simulation of large-scale structure formation including acceleration of CR electrons at cosmological shocks and magnetic field evolution. Our results are in accord with the observed radio synchrotron and X-ray thermal bremsstrahlung fluxes. Thus we conclude that the reported radio detection is the first evidence of cosmic-ray particle acceleration taking place at cosmic shocks in a magnetized inter-galactic medium over scales of $\gtrsim 5\, h_{50}^{-1}$ Mpc.

Key words: Acceleration of particles; Cosmic rays; Cosmology: observations; Galaxies: clusters: general; Large-scale structure of universe; Magnetic fields; Methods: simulations; Radio continuum: general; Shock waves
PACS: 98.65. r; 98.80.Es; 98.70. f; 98.70.Sa; 95.75. z; 95.85.Bh

1 Introduction

Recent advances in observational cosmology have revealed that the large-scale distribution of galaxies in the Universe has a honeycomb-like structure, where the principal morphological elements are interconnected networks of large filaments and sheets of galaxies surrounding huge regions almost devoid of galaxies (the 'voids') (Einasto et al. 1997, Bond, Kofman & Pogosyan 1996, Doroshkevich et al. 1996). The enduring quest has been to understand how such diverse structures emerge out of primeval density fluctuations that grew over time due to the effects of gravity.

An important role in the structure-formation process is played by the large-scale shocks that form as the primordial density fluctuations become non-linear and the accretion flows on collapsing structures become supersonic (Quilis, Ibnez, & Saez 1998, Miniati et al. 2000, Enßlin et al. 2001). Likely these shocks are responsible for heating of most of the diffuse intergalactic medium (IGM) up to $\approx 10^{5-7}$K (Cen & Ostriker 1999). Given their large sizes and long lifetimes, these shocks have also been proposed to be the sites for the acceleration of very high energy cosmic-rays up to $10^{18} - 10^{19}$ eV (Norman, Melrose & Achterberg 1995, Kang, Ryu, & Jones 1996). In addition, it has been recently pointed out that the cosmic-ray ions accelerated at intergalactic

[1] E-mail addresses: joydeep@iucaa.ernet.in (Bagchi),
ensslin@mpa-garching.mpg.de (Enßlin),
fm@mpa-garching.mpg.de (Miniati),
stalin@upso.ernet.in (Stalin), msingh@upso.ernet.in (Singh),
somak@star.sr.bham.ac.uk (Raychaudhury), deephum@yahoo.com (Humeshkar).
[2] Present address: School of Physics, University of Hyderabad, Hyderabad 500046, India.
[3] Corresponding author. Fax: +91-20-5690760. e-mail: joydeep@iucaa.ernet.in

shocks could accumulate in the formed structure, storing a significant fraction of the total energy there (Miniati et al. 2001a). Exploration of such ideas through direct observations is truly important because even after close to a century since cosmic-rays were discovered by Victor Hess in 1912, we do not know how and where they are accelerated.

Direct evidence for the ability of cosmic shock waves to accelerate particles is given by the observed association of the so called 'cluster radio relic' sources with locations where shock waves are expected from X-ray observations (Enßlin et al. 1998). Diffusive shock acceleration may be operative at these locations and responsible for the radio emitting electrons. But also shock reillumination of fossil radio plasma in remnants of former active radio galaxies is a viable explanation (Enßlin & Gopal-Krishna 2001). The latter mechanism seems to be the explanation of at least some of the cluster radio relics, since in some cases very filamentary and torus-like morphologies could be resolved. Such morphologies are predicted by numerical simulations of the shock passage of a fossil radio plasma bubble (Enßlin & Brüggen 2002). However it is quite possible that some of the cluster radio relic sources are caused by diffusive shock acceleration of thermal electrons (Miniati et al. 2001b).

In order for particles to be accelerated, magnetic fields have to be present at the shock waves. Magnetic fields are observed in the intra-cluster medium (ICM) of clusters of galaxies by Faraday rotation of polarized background sources (Clarke, Kronberg, & Böhringer 2001). They are further revealed by the presence of cluster-wide Mpc scale radio halos in some clusters of galaxies, believed to be the result of synchrotron emission of relativistic electrons accelerated in magnetic fields. The role of the magnetic fields in clusters is still a matter of debate, but some recent works indicate important dynamical influences in the ICM (Clarke, Kronberg, & Böhringer 2001, Vikhlinin, Markevitch, & Murray 2001). Outside clusters, no firm detections of magnetic field in the intergalactic medium (IGM) has yet been reported to our knowledge, but speculations on the magnitude of magnetic fields in IGM range from 10^{-7}G to 10^{-12}G.

The origin of cosmic magnetic fields is currently unknown and for this reason any observational evidence of them in the IGM environment is of great importance. Magnetic fields could have a primordial origin or they could have been seeded and amplified during the relatively recent history of large scale structure formation. In this latter scenario, the Biermann battery mechanism (Biermann 1950) operating at either large-scale shocks (Kulsrud et al. 1997, Ryu, Kang & Biermann 1998) or ionization fronts (Gnedin et al. 2000) has been proposed as a viable model for generating seeds of strength $10^{-19} - 10^{-23}$G, to be subsequently amplified by turbulent motions and/or galactic dynamos up to μG level. Alternatively, the origin of cosmic magnetic fields has been attributed to the pollution of the inter-galactic medium by winds and out-

flows from primeval galaxies (Kronberg et al. 1999) and/or quasars and radio galaxies (Furlanetto & Loeb 2001, Gopal-Krishna & Wiita 2001). In most of these cases, magnetic fields would be expected to be present not only inside galaxy clusters, but also in filaments. There were earlier attempts to estimate the magnetization of the Universe from quasars (Daly & Loeb 1990, Medina-Tanco & Enßlin 2001).

The detection of magnetic fields in the IGM outside clusters of galaxies would help the understanding of the origin of magnetic fields within galaxies and galaxy clusters. At the same time, observational evidence for cosmic-rays in the intergalactic medium would allow us to further our understanding of high energy phenomena occurring in cosmic structures which have recently received much attention [see *e.g.,* Feretti & Giovannini (1996) and references therein]. Observationally exploring these issues would provide important clues for many physical problems, including, among others, the theories of ultra-high energy cosmic-ray acceleration and their intergalactic propagation, the origin of radio and hard X-ray emission from galaxy clusters, and the contribution to the diffuse gamma-ray background from shock-accelerated TeV cosmic-ray electrons (Loeb & Waxman 2000).

In this paper we report on the observational evidence of large-scale diffuse radio synchrotron emission (§ 4) over an extended region around ZwCl 2341.1+0000, which is likely to be a proto-cluster of galaxies containing several large filaments (§ 3). The ROSAT X-ray observation of this structure is presented in § 5. The result of a search for association of ZwCl 2341.1+0000 with other galaxy concentrations on a super-cluster scale is reported in § 6. Our observations imply the existence of magnetic fields and relativistic electrons at GeV energies over scales of several Mpc (§ 4 & § 7). The observed radio emission is compared with theoretical predictions from analytical (§ 7) and numerical modeling (§ 8) of particle acceleration at structure formation shocks. Finally in § 9 we discuss the implications of our results and the outlook for future work.

Unless stated otherwise, we adopt an $\Omega_m = 1$ Einstein-de Sitter cosmology and the Hubble constant $H_0 = 50\,h_{50}\,\mathrm{km\,s^{-1}\,Mpc^{-1}}$. The angular scale is $330\,h_{50}^{-1}$kpc per arcminute at a redshift z=0.3. The radio spectral index α is defined such that flux density F_ν is a power-law $F_\nu \propto \nu^\alpha$.

2 The ZwCl 2341.1+0000

The multi-Mpc scale filamentary network of galaxies in ZwCl 2341.1+0000 was discovered in an ongoing program to search for the large-scale diffuse radio emission ($\sim 1\,$Mpc or larger) originating in distant clusters of galaxies.

The primary aim of this program is to investigate the origin and evolution of high energy relativistic particles and magnetic fields in the IGM of large cosmic structures. To this end, we searched for the presence of diffuse radio emission in the field of several Abell and Zwicky clusters or groups with measured/estimated redshifts $\gtrsim 0.15$. Although not a statistically complete sample, it nevertheless contains many clusters that have no detailed information available so far. As a first step, we searched for radio emission in the 'New VLA All Sky Survey' (NVSS (`http://www.cv.nrao.edu/nvss/`)) images at the 1.4 GHz frequency (Condon et al. 1998). The NVSS survey uses the VLA's most compact D-array configuration and is well suited for detection of large structures of angular scales up to ~ 15 arcmin in extent. The completeness limit for point sources is about 2.5 mJy and the angular resolution (beam size) is about 45 seconds of arc.

In the NVSS data, we discovered, among others, a large-scale diffuse emission feature in the region of galaxy concentration ZwCl 2341.1+0000 located at R.A. $23^h43^m39^s.7$ Dec. $+00°16'39''$. It is classified as a distant group 5 or "extremely distant" cluster with cluster diameter $22'$ by Zwicky et al. (1961-68)). Further literature and data search with the NASA Extragalactic Database (NED (`http://nedwww.ipac.caltech.edu`)) showed no additional information on this concentration of galaxies. However, the optical images of the Second Generation Palomar Digitized Sky Survey (DSS-2 (`http://archive.eso.org/dss/dss`)) revealed a very interesting cosmological scale (projected size ~ 25 arcmin or $8h_{50}^{-1}$Mpc) filamentary network of faint galaxies, which had the distinctive non-relaxed morphology of a forming structure. Motivated by these findings, and with an aim to investigating the physical properties of this object in greater detail, we obtained several more detailed observations at radio and optical wavelengths. These observations and the results of their analysis form the subject matter of the following sections.

3 Optical data

3.1 CCD imaging and analysis

We obtained several deep optical and NIR images with the 1-m Carl-Zeiss reflector at the State Observatory, Nainital, India, in November 1999. Due to constraints of time and scheduling, only data in Johnson V, R, and I filters were obtained using a CCD camera equipped with a 2K $\times$ 2K pixels chip, giving a plate scale of 0.37 arcsec/pixel, and a field of view of about 13 arcmin at the f/13 Cassegrain focus. The gain and the read-out noise were 10 e^-/ADU and 13.7 e^- respectively. The sky conditions during the observations were photometric but the seeing was moderate at $\sim$2 arcsec FWHM. We took

several frames in each filter with total exposure time sufficient for adequate photometric accuracy. Photometric zero points and colour transformations were defined by observing Landolt standards. The initial optical processing of the CCD frames was done using the IRAF software and the final object detection, magnitude evaluation and object (star/galaxy) classification was performed using the 'SExtractor' image analysis program (Bertin & Arnouts 1996).

The resulting source catalogue contains a total of 271 galaxies detected to a magnitude limit of $m_V = 21.9$, $m_R = 20.9$, and $m_I = 20.2$, and which were detected independently in all three passbands. The total magnitudes for galaxies at the faint end had typical errors of ∼0.05–0.10 mag. The extinction corrections are small ($A_B < 0.1$ mag over the area of observation) due to the high galactic latitude ($b = -58°$) position. The parameters for the extinction were obtained from the IRAS based galactic extinction estimates by Schlegel, Finkbeiner & Davis (1998). The astrometric conversion from the pixel to equatorial co-ordinates was performed with IRAF employing several bright astrometric stars identified on the CCD images.

3.2 Optical morphology and luminosity

The Fig. 1 shows the *R*-band co-added image of the galaxy concentration. Morphologically it is best described as a long S-shaped main filament of galaxies extending over 12 arcmin ($\sim 4h_{50}^{-1}$ Mpc, which is the size of the CCD frame), and branching structures of several Mpc-scale galaxy sub-filaments mainly to the east and north-east of the main chain. The photometric redshift estimate places the structure at a redshift of z≈ 0.3, supported by spectroscopic evidence from the SDSS survey (see §3.4 below).

If the entire structure is actually a web-like formation at a single redshift and not an artifact of projection (evidence in support of this is presented below), the implications are clearly very important. The branching chain structure and multiple peaks in the galaxy distribution might indicate hierarchical merging of cosmic structures distributed on Mpc scales, at a moderately high redshift. This type of structure is to be expected in evolving Universe according to the "cosmic web" theory of structure formation (Bond, Kofman & Pogosyan 1996), and it is frequently seen in computer simulations such as the the Hubble-volume N-body simulation (Colberg et al. 2000), and also in observational surveys such as the Las Campanas redshift survey (Doroshkevich et al. 1996). These results predict that matter in the Universe should be concentrated along filaments, and clusters of galaxies should be found where these filaments intersect. It is interesting to note that the filamentary morphology of ZwCl 2341.1+0000 is quite similar to a more distant proto-cluster

RX J1716.6+6708 at $z = 0.81$ (Henry et al. 1997).

The average integrated galaxy V luminosity of 12 randomly selected positions on the main filament and side chains, after correcting for the local background offset from main structure, yields a value of $2.7 \times 10^{11} L_{\odot}/\mathrm{arcmin}^2$ ($\pm 54\%$) for the observed average luminosity of the filament. The indicated dispersion about the mean value represents the fluctuation of the surface brightness occuring over the galaxy filaments, rather than the uncertainty of measurement.

3.3 Galaxy colours & estimating photometric redshifts

We estimated photometric redshifts for the galaxies in our catalogue to ascertain the mean redshift of the concentration, and to verify that most of the galaxies projected on the sky plane near this concentration represent an association in real space. This method is a powerful tool for detecting high spatial density regions such as clusters and groups and has recently been applied to the study of galaxy populations in high-z clusters of galaxies (Lubin et al. 2000, Gladders et al. 1998). From our photometric catalogue of galaxies in V, R and I bands, a set of 6 plots; three of colour-magnitude (C-M) diagrams and three of colour-colour (C-C) diagrams, were generated. Figs. 2 & 3 show the $(V-I)$ and $(R-I)$ colours vs. I magnitudes for all the galaxies. On both planes, a well defined linear sequence of early-type (E/S0) galaxies is clearly visible.

Early-type galaxies form the dominant population in cores of all clusters, rich or poor, and across a wide range of redshifts, low to $z > 1$ (e.g., Gladders et al. (1998)). Their ubiquitous colour-magnitude sequence, first noted locally by Baum (Baum 1959), is now well documented in many clusters, ranging from Coma to clusters at redshifts up to $z = 1$ (Stanford, Eisenhardt, & Dickinson 1998, Ellis et al. 1997, Gladders & Yee 2000). The colours of elliptical galaxies become bluer as they become less luminous. We have detected this red C-M sequence on all three C-M diagrams, which shows that at least the dominant galactic population consists of early-type galaxies that are part of this filament at a single redshift. This is a good indicator of association of galaxies in a large-scale structure, as a random projection of field galaxies can not generate the red sequence which is characteristic of clusters. On the C-M diagrams, apart from E/S0s, a population of blue galaxies (late spirals and irregulars) can also be seen in the lower-right region.

From the position of each galaxy in a 3-dimensional colour space, consisting of orthogonal axes $(V-R)$, $(V-I)$, and $(R-I)$, the three colour-colour diagrams were obtained. These diagrams can be used to identify the galaxies of various Hubble types and to obtain the redshifts. The Fig. 4 and Fig. 5 show two of

these projections that show galaxies of very wide range of colours. A distinct cluster of data points near $(V-R)=0.9$, $(V-I)=1.6$ and $(R-I)=0.7$ can be seen on these plots. These identify a coeval population of red galaxies of early Hubble types at a single redshift. Therefore, we have further proof that ZwCl 2341.1+0000 is indeed a real concentration of galaxies.

The properties of the galactic populations in these filaments were investigated using the spectrophotometric evolutionary models of Guiderdoni & Rocca-Volmerange (1988). These models give evolutionary synthetic spectra for a number of spectral classes reproducing the range of spectrophotometric properties for the Hubble sequence. From this work, the data on predictions for apparent magnitudes and colours of galaxies of wide range of redshifts were obtained and fitted to the observed colours and magnitudes. The evolutionary tracks, representing the redshift evolution of galaxy colours, were plotted on the colour-colour diagrams. The data included the effects of K-correction, evolutionary correction and of the emission of nebular component plus the correction for internal extinction (see Guiderdoni & Rocca-Volmerange (1988) for exact details). The colours of E and S0 galaxies are useful in determination of redshift because of the uniformity of their spectral properties and because of a large 4000 A° break due to the Balmer edge in their spectra provides the strongest signal for photometric redshift estimation. In Fig. 4 and Fig. 5 it is apparent that the evolutionary tracks for the early type E/S0 galaxies fall closest to the observed data cluster at redshift $z \sim 0.3$. The colours for E/S0's at redshifts $z=0.2$ or $z=0.4$ both showed a much poorer fit to the data, particularly on the $(V-I)$ vs. $(V-R)$ plot which has the steeper slope.

To avoid projection effects, the actual fit of the spectrophometric model colours to the observed data was performed in a 3-dimensional colour space. At redshift $z=0.3$, the model colours for the E/S0 galaxies are: $(V-R)_{mod}=0.92$, $(V-I)_{mod}=1.58$, and $(R-I)_{mod}=0.66$. Enclosed within a sphere of radius 0.30 colour index units centered on the model point, we found an agglomerate of 79 data points. These are the likely to be the E/S0 galaxies (having similar colours) that have high probability to belong to the filament. The radius of 0.30 colour-index units takes into account the intrinsic spread in colours of E/S0 galaxies observed in clusters. The plotted position of these galaxies on the C-M diagrams (Fig. 2 and Fig. 3) forms well defined linear sequences characteristic of early type galaxies in clusters, confirming that they are E/S0 galaxies. The mean and standard deviation of these galaxy colours were calculated as: $(V-I)_{E/S0}=1.59\pm0.12$, $(V-R)_{E/S0}=0.88\pm0.09$, and $(R-I)_{E/S0}=0.72\pm0.11$. Clearly, the model for E/S0 galaxies fits the cluster photometric observations quite well (within $\lesssim 0.5\sigma$). From this evidence it was estimated that the actual redshift is $z=0.30\pm0.05$, which was used in all our analysis and interpretation. A more sophisticated analysis aiming at greater precision was not attempted as the accuracy of the redshift estimate was limited by the availability of only three photometric colours. The accu-

racy of the photometrically estimated redshift is sufficient for the purpose of the present paper. In addition, the plotted template colours for the galaxies of Hubble types Sa, Sb, Sc, Sd and Irr at $z = 0.3$ fitted the data well, as can be seen in Fig. 4 and Fig. 5, providing independent verification of the redshift estimate.

3.4 Spectroscopic redshifts

The current release of the ongoing Sloan Digitized Sky Survey (York et al. 2000) includes the spectra of four of the galaxies in our catalogue, from which redshifts are shown in Table 1. The location of these galaxies are shown by arrows in Fig. 1. The mean redshift from these four galaxies, $z \sim 0.267$, is consistent with our photometric redshift estimate in the previous section. For the rest of paper, we will assume the redshift of the filamentary structure to be $z = 0.3$.

Table 1
Spectroscopic redshifts from the SDSS

Galaxy no.	R.A. J(2000)	Dec. J(2000)	Magnitude	Redshift
1	$23^h43^m38.2^s$	$00°19'46''$	18.9	0.272093
2	23 43 40.7	00 20 30	17.6	0.260870
3	23 43 34.6	00 20 37	18.0	0.269087
4	23 43 21.7	00 19 33	17.7	0.266947

4 The radio observations

4.1 The low resolution VLA (NVSS) radio data at 20 cm

The 1.4 GHz (λ =20 cm) radio map obtained from the NVSS (`http://www.cv.nrao.edu/nvss/`) archives is shown superposed on the optical R-band CCD image in Fig. 6. The original data of 45 arcsec (FWHM) resolution was convolved with a Gaussian to obtain a 60 arcsec (FWHM) resolution beam in order to better detect the large-scale diffuse emission regions. The 1σ noise level on this image is within range $\approx 0.5 - 0.6$ mJy/beam, whereas on the unsmoothed original image it was ≈ 0.45 mJy/beam.

Morphologically, the source appears to have a complex structure, but mainly consisting of two parts: the southern section (at R.A. $23^h43^m49^s$, Dec. $00°14'14''$)

is $\approx$ 5 arcmin (1.65 h_{50}^{-1}Mpc) in size and is entirely diffuse in nature, and the peak emission here is about 4 mJy/beam. The northern section (at R.A. $23^h43^m39^s$, Dec. $00°18'44''$), of similar $\approx$5 arcmin angular size, shows evidence of both diffuse and localized radio emissions. Within the northern radio structure, the data allows to resolve two more radio components which are henceforth called for convenience NN (the northern peak of 6 mJy/beam) and NS (the southern peak of 11.5 mJy/beam). The integrated flux density, position and spectral index for various regions of the source are reported in Table 2. The spectral indices were calculated by convolving the NVSS radio map to the broader resolution of the 320 MHz radio map discussed below. A faint 'radio-bridge' type extension at R.A. $23^h43^m43^s$, Dec. $00°16'31''$ between the two sections is an interesting feature. The surface brightness of this 'radio-bridge' is about 1.5-2.5 mJy/beam and therefore it is detected at the level of about 3-4 σ. A strong curvature in the main filament of galaxies can be clearly seen in this region. However, the curved section is not located on the radio-bridge but shifted about 1.5 arcmin to the NE of it. We note that this pattern is again reproduced in the ROSAT X-ray map (Fig. 11) which is discussed in better detail in § 5.

More significantly, the entire structure visible at radio wavelengths is of very large extent (at least 10 arcmin or 3.3 h_{50}^{-1}Mpc) and appears to be roughly aligned with the main optical galaxy filament which is of similar size. Thus the radio and optical structures are possibly related and co-spatial. We show below, from high resolution radio data, that only one elliptical galaxy could be associated with a radio peak. The rest of the radio emission therefore possibly originates from diffuse synchrotron radiation (as inferred from the radio spectrum) from the inter-galactic medium.

4.2 High resolution VLA 'FIRST' image and optical identification of possible point sources

The VLA low resolution 20 and 90 cm radio images discussed here have only the modest resolutions of $\sim$1-1.8 arcmin, while in a portion of sky covered by a galaxy cluster there can be several hundred galaxies. It is therefore possible that a significant part of the radio emission could arise from the blend of radio sources in the cluster (and distant background point sources). It is therefore very important that we should identify the regions of genuine large-scale diffuse emission from superposed point sources. To check for this serious source of confusion, we have cross correlated the optical ZwCl 2341.1+0000 cluster field with the NRAO 'FIRST' (`http://sundog.stsci.edu/first/description.html`) radio catalogue. The 'FIRST' survey, conducted with the VLA B-configuration, contains high resolution ($\approx$ 5 arcsec beam) radio maps at 1.4 GHz with a flux density threshold of 1 mJy and a typical rms of 0.15 mJy/beam. The astro-

Table 2
Radio data

Region	R.A. J(2000)	Dec. J(2000)	S_{320} mJy	S_{1400} mJy	Ang. size (arcmin)	Sp. indx. α_{320}^{1400}
North half(total)[a]	–	–	50 ± 10	28 ± 2	~ 5	-0.40 ± 0.20
NN[a]	23 43 39.9	00 20 53	22 ± 5	11 ± 2	~ 2	-0.47 ± 0.20
NS[a]	23 43 39.4	00 18 41	28 ± 5	17 ± 2	~ 2	-0.34 ± 0.15
South half[a]	$\sim$23 43 49	00 14 14	42 ± 8	20 ± 2	~ 5	-0.50 ± 0.15
Extended 90 cm[b]	$\sim$23 44 03	00 22 00	36 ± 10	< 10	~ 4	< -0.9
Total source	–	–	128 ± 16	48 ± 5	~ 12[c]	
Radio Power[d]	–	–	5.6 ± 0.7	2.1 ± 0.2	–	–

a: As defined in the VLA 1.4 GHz observations. b: The excess diffuse emission found with VLA 320 MHz data. c: The largest angular size at 320 MHz. The size measured along the 'ridge-line' is about 18.4 arcmin. d: The total monochromatic radio power in units of $10^{25}\, h_{50}^{-2}$ W Hz^{-1}.

metric reference frame of the maps is accurate to 0.05 arcsec and individual sources have 90% confidence error circles of radius < 0.5 arcsec at the 3 mJy level. To achieve an equivalent degree of precision, for optical identification we have used the Palomar Digitised Sky Survey (DSS-2) red sensitive plate for which the astrometric accuracy is better than ± 0.5 arcsec r.m.s. With such good radio and optical astrometric precision, it is possible to identify superposed point sources, if any are present. We note that the large-scale structures $\gtrsim 30$ arcsec angular size are resolved out by the FIRST survey, but compact features, such as unresolved radio-cores or jets, can be easily identified.

Fig. 7 shows the FIRST image (contours) superposed on the DSS-2 image (gray scale) for optical identification of radio sources. The image covers the northern section of the radio filament detected by the NVSS. FIRST survey finds radio counterparts at the position of the two northern sources NN and NS (see § 4.1 on the NVSS data), but the southern region of diffuse emission is completely resolved out and shows no compact radio peak. Similarly, the extended large-scale diffuse emission detected in the 320 MHz data (discussed below) also does not show any point components in the FIRST data. The integrated flux densities of the two sources detected by FIRST are: in the northern source NN 1.8 ± 0.4 mJy and in the southern source NS 9.3 ± 0.6 mJy. The integrated flux densities of the same two sources mapped by NVSS are: in the northern source NN 11 ± 2 mJy and in the southern source NS 17 ± 2 mJy (see Table 2). Clearly, this indicates that while FIRST is actually able to map the regions close to peak emission in both theses sources, there is considerable amount of diffuse emission associated with both which is largly resolved out due to lack of short interferometric spacings (as expected of VLA B-array data). We note

that even with this limitation the FIRST map of the southern radio source NS shows a diffuse morphology and some hints of partially resolved internal structure consisting possibly of two parallel filaments ≈ 6 arcsec apart. These features can be better seen on the detailed radio image shown in Fig. 8. We need more sensitive radio maps to better understand what these features really are.

No object classified as a galaxy with the CCD data could be located on the stronger southern radio peak NS. A faint $m_v = 20.81$ galaxy (G1) was located 6.2 arcsec to the north of the radio peak (Fig. 7), and another brighter $m_v = 18.21$ galaxy (G2) 6.5 arcsec to the south-east direction, but their identification with the radio source is doubtful. The combined radio and optical positional errors correspond to an error circle of radius 1 arcsec and both galaxies are shifted by $\approx 6\sigma$s from the radio peak. The photometric colours of galaxy G1 are quite red and not consistent with those of a standard elliptical galaxy at $z = 0.3$, but are more like those of a higher redshift galaxy. Thus based on high resolution radio and optical data we can not find any good optical identification for this source. Most likely the diffuse source NS is part of the overall large-scale radio filament.

Near the weaker northern radio source NN, an E/S0 galaxy (G3) of magnitude $m_v = 18.19$ could be located at R.A. $23^h\ 43^m\ 40^s.4$, Dec. $+00^\circ\ 20'\ 54''$, poitioned only 1.7 arcsec east from the FIRST radio peak. Due to its close proximity and consistent photometric colours (for redshift z$\approx$ 0.3), we consider it to be a possible candidate host galaxy/AGN for the origin of northern radio peak. At present the true relationship of this weak radio peak with the rest of the extended diffuse emission found with NVSS and 320 MHz data is not very clear. The NVSS map shows an extension of about 2 arcmin size to the west of the radio peak, whereas the 320 MHz map shows both this extension as well as another 'plume' to the east of radio peak NN. We consider two possibilities: first, that the optical galaxy G3 (with a weak radio nucleus) is just superposed on the rest of the radio filament which is not directly related to this galaxy. This possibility can not be ruled out from the present data. Second, that this galaxy is the source of all the radio emission in the region of the source NN. If this is true then can this radio source be a 'head-tail' type radio galaxy commonly found in clusters ? This interpretation is not fully supported by radio spectral index $\alpha_{320}^{1400} = -0.47 \pm 0.20$ as reported in Table 2. The spectral index is quite flat for a head-tail radio source which generally have their integrated spectral indices quite steep $\lesssim -0.7$. On the other hand the fairly flat spectral index of -0.47 is consistent with the similar flat radio spectra noted over the other regions of the radio filament (Table 2). In that case the radio spectral evidence suggests that both the northern sources NN and NS could be local regions of stronger emission embedded within the large radio filament. The cause could be that the physical conditions differ from place to place within the filament, with local effects on particle acceleration

which then is reflected in the intensity of radio emission.

Apart from this possible radio source, no other optical galaxy could be identified with any part of the extended diffuse radio emission mapped by the VLA at 20 and 90 cm wavelengths. Therefore, given the evidence at hand, we consider it to be unlikely that a major part of the large-scale radio structure is due to the blend of radio-galaxies in the cluster or in the background. It is very likely that the radio emission originates entirely in the diffuse intracluster medium and derives its power from an energetic process spread across a region several Mpc wide.

4.3 The meter-wavelength 320 MHz VLA image and spectral indices

The field of ZwCl 2341.1+0000 was further observed by the VLA on May 12, 2000 at 327 MHz ($\lambda = 90$ cm) for a total on-source duration of 2.2 hr. The compact C-array observation was obtained with an aim to achieving resolution and large-scale structural mapping sensitivity comparable to the NVSS data. The two IFs (intermediate frequencies) were centered at 327.5 MHz (IF1) and 321.5 MHz (IF2) with bandwidths of 3.12 MHz in each IF. The data were obtained in spectral-line mode and amplitude (flux density) calibration was obtained by boot-strapping to 3C 48 which was assumed to have a flux density of 42.547 Jy and 42.966 Jy at IF 1 and 2 respectively. The 327.5 MHz data was found to be heavily contaminated by radio interference and therefore could not be used. The quality of 321.5 MHz data was found to be satisfactory and it was used for further analysis. For analysis we used the NRAO 'AIPS' package.

Low-frequency radio imaging of faint sources is always challenging due to large primary beam area of antennae, resulting in detection of many strong sources over this area. In addition, the effects of sky-curvature can not be neglected in mapping and cleaning of fields measuring several degrees in size. In order to mitigate these problems as much as possible, we used the task 'IMAGR' that permits the 'faceted' wide-field mapping and cleaning option. We mapped upto 53 small fields (facets) centered on strong sources located *a priori* within the 5.6×5.6 deg^2 field of view centered on ZwCl 2341.1+0000, and then simultaneously cleaned the entire set. At the end of cleaning cycle the clean components from all facets together were restored back onto a single field to generate a large wide-field image. We point out that due to the use of separate tangent point for each field, 3-D imaging, and the subtraction of clean components from un-gridded data (preventing aliasing of side-lobes), the quality of the final clean image is fairly good. In order to emphasise the large-scale features and supress the oscillations in the side-lobes, the visibility data were tapered by a Gaussian that had 30% weight at the 2 kλ length of the interferometric spacing. This has resulted in better detection of faint

diffuse features, but at the cost of angular resolution which is now 108 arcsec FWHM (circular Gaussian) on the radio map shown in Fig. 9 . The level of background noise on the cleaned image is about 2.5 mJy/beam r.m.s. as against 1.3 mJy/beam expected from pure thermal noise. This about factor 2 higher noise is mainly the effect of residual low-level side-lobes of several strong sources of 0.2 Jy-1.5 Jy flux density occuring nearby that limit the dynamic range achievable to ≈ 400.

In order to facilitate a comparison of the radio maps at 320 MHz and NVSS map at 1400 MHz, we also show two wide-field images covering identical 1.5×1.5 deg^2 fields. The contour levels shown are in multiples of $\sim 1\sigma$ noise on each map. For a better comparison, the original NVSS map has been convolved with a Gaussian to obtain a broader final beam size of 90×90 arcsec^2. These images can be accessed on-line by linking to this address (`http://www.iucaa.ernet.in/ joydeep/vla/`).

Comparison of 90 cm radio map (Fig. 9) with the 20 cm map (Fig. 6) reveals the detection of all the features present on the 20 cm map, albeit at a coarser resolution. Furthermore, starting from radio source NN (in the northern half of 20 cm image) and extending ≈ 5 arcmin to its east, an excess region of diffuse emission can be detected at 90 cm. This can be found at R.A. $\approx 23^h\ 44^m\ 03^s$, and Dec. $\approx 00°22'00''$. Although the reality of features detected both at 20 cm and 90 cm are not in any doubt, we nevertheless introduce a caveat on the excess diffuse radio feature. Although the $\sim 1\,h_{50}^{-1}$Mpc sized 'plume' to the east of radio peak NN does suggest some connection, but it is quite faint and detected at the significance level of about 2σ (surface brightness ≈ 5 mJy/b) only. Therefore it must be treated with due caution. The two radio peaks of diffuse emisiion, further towards east, that also seem to be linked with the plume, are somewhat better detected at the levels of 3σ (peak 7.7 mJy/b) and 5.6σ (peak 14 mJy/b). But due to faint nature of these radio structures, they should also be treated with caution until confirmed with stronger signal in an improved observation. In case these features are real, they would make the total radio size much larger than what is visible at 20 cm wavelength (see below).

The optical morphology of galaxies underlying the 90 cm extended structure is shown in Fig. 10, where the radio contours are shown superposed on the Palomar DSS-2 red sensitive photograph. From this image, and also from the higher resolution 'FIRST' radio data discussed above, no galaxy was found to be apparently associated with any region of the diffuse radio structure.

The largest observed angular size at 90 cms is about 12 arcmin, which corresponds to a projected dimension of $\approx 4\,h_{50}^{-1}$ Mpc. The size when measured along the spine of the filamentary structure was found to be about $6\,h_{50}^{-1}$ Mpc, thus making it comparable or larger than some of the largest known radio

structures in the Universe: the giant radio galaxies 3C236 ($5.8\,h_{50}^{-1}$ Mpc) and NVSS 2146+82 ($3.9\,h_{50}^{-1}$ Mpc) (Strom & Willis 1980, Palma et al. 2000), and also the largest known radio-loud quasar HE 1127-1304 ($2.4\,h_{50}^{-1}$ Mpc; Bhatnagar et al. (1998)). However, there is no evidence available to show that the radio emission in any way constitutes a giant radio galaxy (see § 4.4 below). A peculiar radio morphology and the pronounced lack of symmetry in the observed structure are particularly noticeable in this source.

The extended region was detected at a significance level of 2–5σ. Therefore, for the extended part, the radio spectral index is steep ($\alpha < -0.9$), estimated from its non-detection at 20 cm to the flux density limit of 10 mJy. Estimates of flux densities and the spectral indices for the various regions of the radio structure are listed in Table 2. The overall negative spectral indices in all regions ($\alpha \lesssim -0.5$) indicate a non-thermal mechanism for radio emission, most likely the synchrotron radiation of relativistic charges accelerated in a magnetic field. Therefore it is necessary that both the particles and fields, distributed on similar spatial scales, should be present to generate the radio emission. *To our knowledge, this is the first observational evidence of distribution of particles and magnetic fields on spatial scales* $\gtrsim$ 5 h_{50}^{-1} *Mpc.*

4.4 On the possibility of radio source in ZwCl 2341.1+0000 being a giant radio-galaxy

The so-called giant radio-galaxies (GRGs) are a rare class of largest radio sources whose projected linear size between the radio lobes is $\gtrsim$ 1 Mpc. Their other physical characteristics are that they are mostly bi-symmetric, have edge-brightened FR-II (Fanaroff-Riley class II) radio morphology. Their radio power is in the transition zone between FR-I (low-powered systems) and FR-II (high-powered ones). Furthermore, they tend to occur in regions of both low galaxy density and low intergalactic matter density. In view of the extremely large size noted for the radio source in ZwCl 2341.1+0000, we ask– can it be another GRG?

We have several pieces of evidence which seem to rule out this possibility. First, the radio morphology is very peculiar, lacking any semblance of bi-modal or other symmetry or identifiable radio-jets or large-scale radio-lobes as expected of GRGs. Second, on the high resolution 'FIRST' map we do not find any evidence of a compact radio core associated with a centrally located optical galaxy which could be assumed to be the source of the entire radio structure. Third, the projected linear size in the range 4–6 Mpc is very large even by the standards of GRGs. Schoenmakers et al. (2001), in their systematic study of several GRGs found that beyond the linear size of 2 Mpc the number of GRGs cuts-off sharply and sources above this size are extremely rare. There

appears to be a strong luminosity evolution in the GRG population, such that in the majority of them the activity in the central engine is extinguished over the time it takes for the radio-lobes to expand to size $\gtrsim 2$ Mpc. Therefore, the extreme size of the present radio source and its morphological peculiarities suggest that it is not powered by the energy outpouring in the expanding radio lobes. Some other energy generation mechanism spread over the entire radio structure appears to be at work here. We show below that possibly this is diffusive shock acceleration in structure formation flows. It is therefore unlikely that ZwCl 2341.1+0000 is a giant radio-galaxy.

5 X-ray detection in the ROSAT All-sky survey

An X-ray counterpart of the collapsing filament ZwCl 2341.1+0000 can be found in the ROSAT all-sky survey (RASS (`http://www.xray.mpw.mpg.de/rosat/survey`)). Almost the entire sky was surveyed by the PSPC-C instrument on ROSAT in scanning mode over six months in 1990, such that every point in the sky was observed with an effective exposure time of between 117 and 443.9 seconds.

Fig. 11 shows the RASS observation, smoothed with a Gaussian of $\sigma_r = 4$ pixel ~ 1 arcmin, as contours superposed on the optical (Palomar DSS-2 red) image. We have used only the 0.5-2 keV band of the observations to produce the image, since the softer band shows no significant signal in this region (higher background). The r.m.s. level of background noise on the smoothed image is typically 5×10^{-3} counts/s, which was estimated over several nearby regions. The first contour is shown at the level of about 4 σ (21×10^{-3} counts/s) and next contours are spaced linearly in steps of 1 σ. The highest X-ray peak (45.9×10^{-3} counts/s, 9σ detection) in this region is at R.A. $23^h43^m39.6^s$, Dec $+00°19'40.3''$ (J2000). The secondary peak (37.7×10^{-3} counts/s, 7.5σ detection) is at R.A. $23^h43^m44.4^s$, Dec $+00°15'08''$. The positional accuracy of the X-ray data was checked with respect to the optically identified point X-ray sources in the field and was found to be ≈ 15 arcsec as expected of the RASS (Voges et al. 1999).

The net flux in the 0.1–2.4 keV band in the region shown in Fig. 11 is 2.52×10^{-13} erg cm^{-2} s^{-1} ($\pm 43\%$), corresponding to a 3σ detection. A galactic neutral hydrogen column of 3.7×10^{20} cm^{-2} was assumed (Dickey & Lockman 1990), and no k-correction was applied ($< 10\%$). We assumed a gas temperature of $T = 5$ keV in the calculation. At redshift $z = 0.3$, this flux corresponds to bremsstrahlung X-ray luminosity of $1.1 \times 10^{44}\, h_{50}^{-2}$ erg s^{-1}. The largest angular size of the detected X-ray structure is about 8 arcmin ($2.6\, h_{50}^{-1}$ Mpc), comparable to the size of the radio structure. The structure of the X-ray source appears quite non-relaxed, which suggests that this system is possibly undergoing a violent gravitational merger of subclusters. Therefore the ROSAT data

supports the possibility that ZwCl 2341.1+0000 is in fact a systen undergoing structure formation. This is a likely scenario in view of the filamentary morphology of galaxies noted in optical.

Although the RASS detection is not strong enough in order to provide firm inferences, we nevertheless show a spatial comparison between the radio and X-ray emitting plasma by superposing the 327 MHz radio image and the X-ray contours in Fig. 12. Here we can locate the stronger northern X-ray structure in the northern part of the radio filament while the secondary X-ray peak to the south is in the vicinity of the southern diffuse radio structure and both seem to be joined by an X-ray filament/bridge of ~ 2.2 arcmin (730 h_{50}^{-1} kpc) size ($\approx 27 \times 10^{-3}$ counts/s or 5.4σ detection). We note a strong curvature in the main filament of galaxies located about 1.5 arcmin to the east of this X-ray bridge (Fig. 11). This pattern is also visible on the 20 cm radio and optical superposition shown in Fig. 6. Another extended X-ray filament/plume of ~ 3 arcmin (900 h_{50}^{-1} kpc) size, and detected at the $4-6$ σ level, can be found to the east of the northern X-ray peak where several smaller filaments join with the larger main filament of galaxies. Interestingly, both the X-ray peaks as well as the filaments are apparently displaced from the nearby radio peaks (by as much as 1 to 1.5 arcmin - significantly larger than the X-ray positional error). While this clearly indicates that the X-ray emission mechanism can not be the non-thermal inverse Compton radiation, however it can provide a diagnostic tool to probe the physics of the multi-phase (thermal and non-thermal) intracluster medium in comparison with the structure formation simulation results. A similar strong mismatch between the locations of relativistic and thermal plasma is noticeable in the numerical simulation carried out by us in § 8. We defer the discussion on it's physical significance to § 8 where it will be dealt with in comparison with the theoretical model.

6 The large-scale environment

The linear dimensions of the optical and radio structures described here, although quite large, are both restricted by the maximum possible areas that could be imaged with the optical and radio telescopes used. We have no reason to believe that these are not parts of a larger super-structure, which needs to be verified for its important implications. As of now, neither deep wide-field optical images nor extensive redshift measurements are available in order to check whether or not this concentration of galaxies visible in the region of ZwCl 2341.1+0000 is part of a larger supercluster ($\sim$10–100 Mpc) scale structure.

As a step in this direction, we have used the Palomar DSS-2 survey images and the NASA Extragalactic Database NED (`http://nedwww.ipac.caltech.edu`)

to search for other known clusters and groups within a radius of 2 deg ($40\,h_{50}^{-1}$ Mpc) of the center. There are eight identified galaxy concentrations which are listed in Table 3. The two nearest clusters, Abell 2644 and RXC J2341.1+0018, are at much lower redshifts to be associated with ZwCl 2341.1+0000. The other five Zwicky clusters, situated within 40–75 arcmin, are of comparable richness, but their redshifts are not known. However, there is a very rich cluster Abell 2631 (richness class 3, $z = 0.2730$), which is only 1.5 degree ($30\,h_{50}^{-1}$ Mpc) away on the sky and at a comparable redshift, making it a possible association on a super-cluster scale. Deep wide-field imaging and spectroscopy of a large area in the ZwCl 2341.1+0000 region could reveal the true supercluster-scale environment of this large forming structure.

Table 3
Large scale environment: known groups and clusters within 2 degrees ($40\,h_{50}^{-1}$Mpc)

Cluster or group	R.A. J(2000)	Dec. J(2000)	Redshift	Separation (arcmin)
ZwCl 2341.1+0000	$23^h43^m39.7^s$	$+00°16'39''$	∼0.30	0.0
RXC J2341.1+0018	23 41 06.3	+00 18 53	0.110	38.4
Abell 2644	23 41 09.8	+00 05 38	0.069	39.1
ZwCl 2338.3-0022	23 40 51.8	–00 05 22	...	47.4
ZwCl 2343.9+0029	23 46 27.7	+00 45 40	...	51.0
ZwCl 2342.2+0049	23 44 45.7	+01 05 40	...	51.7
ZwCl 2344.9-0025	23 47 27.8	–00 08 20	...	62.2
ZwCl 2345.7+0030	23 48 15.7	+00 46 41	...	75.2
Abell 2631	23 37 39.7	+00 17 37	0.273	90.0

7 Evidence of particle acceleration in shock waves associated with large-scale structure formation

7.1 The necessity of a large-scale particle acceleration process

The radiative life-time ($t_{\rm life}$) of a relativistic electron in a weak magnetic field ($\sim 10^{-7}$ G) is dominated by inverse Compton loss (IC), and it is given by

$$\mathrm{t_{life}} = 80.36 \times 10^6 \ \mathrm{yr} \ \left(\frac{\gamma}{10^4}\right)^{-1} = 4.1 \times 10^7 \ \mathrm{yr} \ \left(\frac{\mathrm{E_e}}{\mathrm{GeV}}\right)^{-1}, \qquad (1)$$

where E_e is the electron energy, γ is the electron Lorentz factor and the redshift is assumed to be $z = 0.3$. At the strongly turbulent magnetic field environment near the sites of particle acceleration (e.g., shocks), the diffusion may be governed by the Bohm approximation, in which the diffusion coefficient is (e.g., Drury (1983))

$$\kappa_{\rm Bohm} = 3.31 \times 10^{23} \left(\frac{E_e}{\rm GeV}\right) \left(\frac{B}{10^{-7}\ {\rm G}}\right)^{-1} \ {\rm cm}^2\ {\rm s}^{-1}. \quad (2)$$

Therefore, the diffusion length-scale ($L_{\rm diff}$) for an electron within the inverse Compton radiative cooling life-time $t_{\rm life}$ is

$$L_{\rm diff} = (\kappa_{\rm Bohm} \cdot t_{\rm life})^{1/2} = 6.7 \left(\frac{B}{10^{-7}\ {\rm G}}\right)^{-\frac{1}{2}} \ {\rm pc}. \quad (3)$$

The linear size of the observed radio emission $L_{\rm radio}$ is about several Mpc which is much bigger than L_{diff}. Therefore, electrons once accelerated in a localized point source such as a radio galaxy or AGN and diffusively transported cannot be the source of the large-scale radio emission. The discrepancy between the Bohm diffusion length-scale and the radio structure size is so large, that even in the case of ordered magnetic fields, where diffusion should be more effective (than in the Bohm approximation), electrons are still unable to cross the emission region within a radiative life-time.

Furthermore, we have not found any evidence of radio jets originating at a central nucleus and transporting bulk kinetic energy to large distances in expanding radio-lobes. Therefore, it is required that the particles (electrons) must be accelerated *in situ*, and the acceleration mechanism should be such that it is extended over scales of several Mpc, and long-lived over the dynamical time-scale $t_{\rm dyn} \sim 10^9$ y. In addition, they are required to be energetic enough to rapidly achieve relativistic energies on an acceleration time-scale t_{acc} such that $t_{\rm acc} < t_{\rm life} < t_{\rm dyn}$. We show below that the diffusive shock acceleration associated with the formation of large-scale structure ZwCl 2341.1+0000 is the most viable mechanism in operation.

7.2 Energetics of shock acceleration and estimates of the magnetic field strengths involved

The extremely large linear size for the radio structure, its peculiar radio morphology unlike any radio galaxy, and its association with this striking optical filament of galaxies, suggest to us that we are possibly witnessing a new and hitherto unknown type of radio phenomenon. The NVSS VLA map

has a central surface brightness of $S_{1.4\mathrm{GHz}} \approx 5.5\,\mathrm{mJy/arcmin^2}$ for the diffuse emission of the source ZwCl 2341.1+0000 ($1\ \mathrm{mJy} = 10^{-29}\ \mathrm{W\,Hz^{-1}\,m^{-2}}$). From radio data, a power-law radio-frequency spectrum with spectral index $\alpha \sim -0.5$ is found in the diffuse parts. Assuming this to be the spectral index across the radio frequency range $\nu_1 = 10$ MHz to $\nu_2 = 10$ GHz, the representative radio surface-brightness of this structure can be estimated to be $Q_{\mathrm{radio}} = 1.6 \times 10^{42}\,\mathrm{erg\,s^{-1}\,Mpc^{-2}}$. Any possible acceleration mechanism should be energetic enough in producing this order of radio brightness over the entire filament.

The mechanism for the radio emission is very likely to be the synchrotron radiation of relativistic charges accelerated in a magnetic field, and therefore the presence of a magnetic field energy is necessary. To obtain an estimate of the field strength in the observed structure, we minimize the total non-thermal energy density, required to produce the observed radio emission, with respect to the magnetic field and write for the minimum energy field [which is close to the equipartition field, (Miley 1980)],

$$\mathrm{B_{me}} = 0.35 \left[\eta\ \sin^{3/2}\phi\ \left(\frac{\mathrm{d}}{\mathrm{Mpc}}\right)\right]^{-\frac{2}{7}}\ \mu\mathrm{G}. \tag{4}$$

Here, we have tacitly assumed an energy ratio of protons to electrons equal to unity, and $\alpha = -0.5$. For a range of volume filling factor η= 1–0.5, and the angle of field lines relative to line of sight ϕ = 90–45 deg, our estimated field spans the range $\mathrm{B_{me}} = 0.5$–$0.3\ \mu$G, assuming a cylindrical geometry with observed length = 3.3 Mpc (10 arcmin), width = 1 Mpc (3 arcmin), and assumed depth $d = 1$ Mpc, consistent with the morphology of the filament as observed at 20 cm. The calculated minimum energy field B_{me} depends weakly on source geometry, the nonthermal spectral index, and the frequency range of the synchrotron radiation, usually taken to be 0.01-100 GHz.

It is more likely, however, that the emission comes from a thin layer close to the accretion shock surface. This implies a much smaller filling factor. If we assume that $\eta = 0.01$ and ϕ = 90–45 deg, the magnetic field obtained is in range $\mathrm{B_{me}} = 1.3 - 1.5\,\mu$G. The radiative age of the 1.4 GHz radio-emitting electrons, undergoing inverse Compton and synchrotron emission losses, is then only $\lesssim 50\,\mathrm{Myr}$.

The diffuse radio emission from a region several Mpc across can only originate in a powerful energy source of a similar size. To our knowledge, only the expected accretion flow of inter-galactic matter onto the filament is sufficiently extended, long-lived, and energetic to overcome the radiation losses of the relativistic electrons over a Mpc-scale filament. The exact physical mechanism of the electron acceleration is yet to be revealed. It is logical to assume, from its filamentary structure and high redshift, that ZwCl 2341.1+0000 is evolving

towards, but is still far from becoming, a centrally condensed galaxy cluster. The accretion shocks associated to forming structures are typically strong, with Mach numbers, $M \sim 5 - 10$, as opposed to the weaker merger shocks which typically have $M \sim 2$ (Miniati et al. 2000). This makes them ideal sites for high energy particle production. Diffuse regions of large-scale radio emission, commonly known as 'radio relics' and 'radio halos', and the detection of temperature structure in several nearby galaxy clusters are possibly related to such shocks (Willson 1970, Kim et al. 1989, Feretti & Giovannini 1996, Deiss et al. 1997, Bagchi, Pislar, & Lima Neto 1998, Lima Neto, Pislar & Bagchi 2001, Enßlin et al. 1998, Giovannini, Tordi, & Feretti 1999, Enßlin & Gopal-Krishna 2001, Miniati et al. 2001b, Enßlin & Brüggen 2002). However, no such evidences have hitherto been found in supercluster-scale filamentary structures at high redshifts.

We propose here that the large-scale radio emission and magnetic field detected in ZwCl 2341.1+0000 are strong evidences for diffusive shock-acceleration (Bell 1978, Blandford & Ostriker 1978) of particles in structure formation flows (Enßlin et al. 1998, Miniati et al. 2001b). A natural consequence of this process would be a power-law spectrum of the momentum distribution. The acceleration process giving rise to a pool of high-energy cosmic-ray particles (both electrons and protons), and specifically the radio emission tracing the radiation from energetic electrons interacting with the magnetic fields. The inverse Compton scatter of cosmic microwave background photons from accelerated electrons may also generate a detectable hard X-ray flux from the structure (e.g., Bagchi, Pislar, & Lima Neto (1998)).

We test the viability of the suggested mechanism by showing that the available kinetic power in the accretion flows in this galaxy filament is sufficient to explain the observed radio luminosity and the unobserved inverse Compton radiation. For this, we consider a simplified model of the filament. The main structure is described as an infinite extended, linear, self-gravitating, isothermal cold dark matter (CDM) filament. The radial profile of the dark matter mass distribution is

$$\varrho_{\rm CDM}(r) = \varrho_{\rm CDM,o} \left[1 + \frac{r^2}{8\, r_{\rm scale}^2}\right]^{-2},$$

where r is the radius, and $r_{\rm scale} = \sigma_{\rm CDM}/(4\,\pi\, G\, \varrho_{\rm CDM,o})^{1/2}$ is the typical scale of the dark matter distribution which has a central density of $\varrho_{\rm CDM,o}$ and a 1-dim. velocity dispersion of $\sigma_{\rm CDM}$. G is the gravitational constant.

The observed galaxies can be regarded as test particles since they do not significantly affect the gravitational potential of the dark matter. Since the galaxies are expected to have a smaller velocity dispersion $\sigma_{\rm gal}$ than the dark matter, we assume a conservative velocity bias of $b_{\rm v} = \sigma_{\rm gal}/\sigma_{\rm CDM} \approx 0.8$ (Carl-

berg, Couchman & Thomas 1990). This leads to a spatially more concentrated profile for the galaxies

$$\varrho_{\rm gal}(r) = \varrho_{\rm gal,o} \left[1 + \frac{r^2}{8\, r_{\rm scale}^2}\right]^{-2/b_{\rm v}^2} .$$

We estimate that the visible diameter of the filament of roughly $D_{\rm gal} = 100$ arcsec corresponds to the region where the projected galaxy density is above 30% of the central value, which implies $D_{\rm gal} \approx 4\, r_{\rm scale}$. As shown in § 3.2, the observed average V-band luminosity of the filament of galaxies is estimated to be $2.7 \times 10^{11} L_\odot/{\rm arcmin}^2$. For a central mass to light ratio of $M/L_V = 100$, this translates into a central dark matter mass density of $\varrho_{\rm CDM,o} = 4.5 \times 10^{-26}\, {\rm g\, cm^{-3}}\, \cos\theta$. Here, θ is the (unknown) angle of the filament axis and the normal to sky-plane, which we assume in the following to be $\theta = 45°$. The velocity dispersion of the dark matter can then be estimated to be $\sigma_{\rm CDM} \approx 690$ km/s.

The estimated high central density and high velocity dispersion of this galaxy filament are comparable to that of a small galaxy cluster. The velocity of the in-falling matter should reach a final velocity of $v_{\rm in} = \sqrt{3}\, \sigma_{\rm CDM} = 1200$ km/s, in order to provide the velocity dispersion of the filament. This estimate of high velocity of infall is in accord with previous estimates based on hydrodynamic simulations (e.g., Ryu & Kang (1997)), and with those derived theoretically (e.g., Bertschinger (1985)). The characteristic incident velocities are $u_s \approx 10^3\, {\rm km\ s^{-1}}\ [({\rm M_{cl}/R_{cl}})/(4 \times 10^{14} {\rm M_\odot/Mpc})]^{1/2}$ in accretion shocks around clusters of galaxies of given mass-to-radius ratio M_{cl}/R_{cl}.

We now estimate the rate of dissipation of kinetic energy by the accretion shock over the surface area of the filament, given by $Q_{\rm kin} = \frac{1}{2}\, \varrho_{\rm gas,in}\, v_{\rm in}^3$. We assume the infalling low density baryonic gas to have a proton number density $n_{\rm P} = 10^{-5}\, {\rm cm^{-3}}$, corresponding to the mass density of $\varrho_{\rm gas,in} = 1.67 \times 10^{-29}\, {\rm g\ cm^{-3}}$ (i.e., $\varrho_{\rm gas,in}/\varrho_{crit} = 3.55$). This gives $Q_{\rm kin} = 1.4 \times 10^{44}\, {\rm erg\, s^{-1}\, Mpc^{-2}}$, which is sufficient to provide an integrated (over the radio spectrum) radio brightness $Q_{\rm radio} \approx 1.6 \times 10^{42}\, {\rm erg\, s^{-1}\, Mpc^{-2}}$ even if this kinetic power is converted to radiative energy with an efficiency of $\approx 1\%$.

In addition, this kinetic power allows for the low general efficiency of the diffusive shock-acceleration process ($\sim 10\%$) and cooling due to inverse Compton radiation $Q_{\rm IC} = 10.5\, Q_{\rm radio}\, (B/\mu{\rm G})^{-2}\, (1{+}{\rm z})^4$. Therefore, balancing the energy gain by $Q_{\rm kin}$ with the losses in the energy-budget, we obtain an upper limit to the inverse Compton loss $Q_{\rm IC} < 1.4 \times 10^{44}\, {\rm erg\, s^{-1}\, Mpc^{-2}}$ and a lower limit to the allowed magnetic field strength in the inter-galactic medium $B \gtrsim 0.56\, \mu{\rm G}$. We note that even lower values of the magnetic field strength are allowed if the available kinetic power is higher than estimated here, either due to a higher infalling mass density or a larger velocity of the accretion flow.

Following Drury (1983), the mean acceleration time scale for electrons to reach a given energy is

$$t_{acc} = \frac{8}{u_s^2}\,\kappa_{Bohm} = 8.36\,\left(\frac{E_e}{GeV}\right)\,\left(\frac{B}{10^{-7}\ G}\right)^{-1}\,\left(\frac{u_s}{10^3\ km\ s^{-1}}\right)^{-2}\ yr, \quad (5)$$

where u_s is the shock speed. Here we have taken the limit of strong shock, so the downstream speed u_2 is related to upstream speed u_1 by $u_2 = u_1/4$, and κ/u = constant. For the diffusion coefficient, once more the Bohm diffusion condition $\kappa = \kappa_{Bohm}$ is invoked. Clearly, $t_{acc} \ll t_{life}$, so in comparison to the radiative loss time scale, the acceleration process is virtually instantaneous. Also, the acceleration time-scale is much shorter compared to the expected life time of shocks $t_{acc} \ll t_{shock} (\sim 10^9 y)$. Under these conditions, the maximum energy attained by electrons in the acceleration process can be calculated by setting the acceleration and cooling times equal ($t_{acc} = t_{life}$), which gives

$$E_{e,max} \approx 2.2\,\left(\frac{B}{10^{-7}\ G}\right)^{1/2}\,\left(\frac{u_s}{10^3\ km\ s^{-1}}\right)\ TeV. \quad (6)$$

Protons are expected to achieve even higher energies due to their far less radiative losses. Thus the cosmological accretion shocks in large-scale forming structures such as ZwCl 2341.1+0000 are indeed capable of accelerating particles to very high energies.

8 Comparison with a numerical model

8.1 Description of simulations

In order to investigate the nature of radio emission and magnetic field presented in § 4 & § 7.2, we carried out a specific numerical simulation of large-scale structure formation that, in addition to the the dark matter and the baryonic components, also follows a passive magnetic field and the cosmic-ray electrons (CREs). In the following we briefly describe the technique employed for the treatment of each of these components.

For the cosmological part we have used an Eulerian, grid based Total-Variation-Diminishing hydro + N-body cosmology code (Ryu et al. 1993). We have adopted a commonly favored Λ + cold dark matter model with the following parameters: total mass density $\Omega_m = 0.3$, vacuum energy density $\Omega_\Lambda = 1 - \Omega_m = 0.7$, baryonic mass fraction $\Omega_b = 0.04$, and normalized Hubble constant $h_{50} = 1.34$ (i.e., $H_0 = 67\,km\,s^{-1}\,Mpc^{-1}$). The initial density perturbations were distributed as a Gaussian random field with a power spectrum

characterized by a spectral index $n = 1$ and "cluster" normalization $\sigma_8 = 0.9$. The dark matter component is described by 128^3 particles, whereas the gas component is evolved on a grid of 256^3 cells. We chose a comoving size for the simulation box $L_{\rm box} = 100 h_{50}^{-1}$ Mpc. Such a size should be large enough to allow the formation of groups and small clusters of galaxies with temperatures up to a few keV.

With the above set up, the size of a computational cell corresponds to about 400 h_{50}^{-1}kpc, a dark matter particle mass to about 8.5×10^8 $h_{50}^{-1} {\rm M}_\odot$, and the spatial and mass resolution to a few times these values respectively. The adopted resolution is somewhat modest. However, it is higher than that characterizing the radio observations. In addition, our tests indicate that coarse grid effects do not affect the simulated electrons and their corresponding radio emission too significantly, which are the primary objectives here.

The magnetic field is treated as a passive quantity, in the sense that its dynamical role on the fluid behavior is completely neglected. The initial magnetic field is set to zero but magnetic field seeds are generated at shocks in accord to the Biermann battery mechanism (Biermann 1950). The field strength is thereafter enhanced by shear flow through stretching and by field compression (Kulsrud et al. 1997). However, even at the end of the simulation, the magnetic field within collapsed structures is well below observational values [see Kulsrud et al. (1997) for further details]. For this reason, the overall field strength normalization is arbitrary. Nevertheless, the simulation will provide important information about the topology and the relative strength of the magnetic field in different regions of the flow.

Finally, the evolution of the CREs is computed by means of the numerical code COSMOCR (Miniati 2001, Miniati 2002). The code is fully described in the given references and here we shall only briefly summarize the salient aspects of it. We suppose that CREs are only injected at shocks from the thermal plasma and we neglect the contribution from any other source (e.g., secondary electrons produced in inelastic p-p collisions, or injected from radio-galaxies). The injection at shocks is parametrized in the following way. We compute the fraction of injected cosmic-ray protons according to the 'thermal leakage' model [*e.g.,* Kang & Jones (1995)], and assume a fixed value $R_{e/p}$ for the ratio of CREs to protons at relativistic energies. This simplified approach, after Ellison, Berezhko, & Baring (2000), is motivated by the fact that the physics underlying the injection at shocks of primary electrons is very complex and not well understood. Observational evidence suggests that this ratio is in the range 0.01-0.05 for the Galactic CRs (Mueller & Tang 1987, Mueller et al. 1995). With the parameters assumed for our 'thermal leakage' model, the fraction of the thermal protons passing through shocks and injected as cosmic-rays is $\sim 10^{-4}$ [see Miniati (2001) for details].

After their injection at shocks as described above, the CREs are evolved taking into account both spatial transport and energy losses/gains. This is achieved by solving numerically a Fokker-Planck equation that has been integrated over finite momentum bins. Basically, momentum space is divided into N_p logarithmically equidistant intervals, referred to as *momentum bins*. The electron distribution function $f(\hat{p})$, as a function of the normalized momentum $\hat{p} \equiv p/m_e c$, in each spatial cell and for each momentum bin is approximated by the following piece-wise power law:

$$f(\mathbf{x}_i, \hat{p}) = f_j(\mathbf{x}_i)\, \hat{p}^{-q_j(\mathbf{x}_i)}, \qquad 1 < \hat{p}_{j-1} \leq \hat{p} \leq \hat{p}_j, \tag{7}$$

where $f_j(\mathbf{x}_i)$ and $q_j(\mathbf{x}_i)$ are the number normalization and logarithmic slope for a given cell and $\hat{p}$ bin. With the above definition, the number density of particles is given by $dN = 4\,\pi\,\hat{p}^2\, f(\hat{p}) d\hat{p}$.

Within each momentum bin j, and at each spatial grid point $\mathbf{x}_i$, we follow the total number density and kinetic energy density of the CREs, defined as

$$n(\mathbf{x}_i, \hat{p}_j) = 4\pi \int_{\hat{p}_j}^{\hat{p}_{j+1}} f(\mathbf{x}_i, \hat{p}) \hat{p}^2 d\hat{p} \tag{8}$$

$$\varepsilon(\mathbf{x}_i, \hat{p}_j) = 4\pi \int_{\hat{p}_j}^{\hat{p}_{j+1}} f(\mathbf{x}_i, \hat{p}) T(\hat{p}) \hat{p}^2 d\hat{p}, \tag{9}$$

where $T(\hat{p}) = (\gamma - 1) m_e c^2$ is the relativistic kinetic energy. Further, for each momentum bin, $q_j(\mathbf{x}_i)$ is determined self-consistently from the values of $n(\mathbf{x}_i, \hat{p}_j)$ and $\varepsilon(\mathbf{x}_i, \hat{p}_j)$ defined above [see Miniati (2001) for details]. With this formalism, the evolution of $n(\mathbf{x}_i, \hat{p}_j)$ in momentum space is described by the equation

$$\frac{\partial n(\mathbf{x}_i, \hat{p}_j)}{\partial t} = -\nabla \cdot [\mathbf{u}\, n(\mathbf{x}_i, \hat{p}_j)] + \Big[b(\hat{p})\; 4\pi\; \hat{p}^2\; f(\hat{p}) \Big]_{\hat{p}_{j-1}}^{\hat{p}_j} + Q(\mathbf{x}_i, \hat{p}_j), \tag{10}$$

where the first term on the right hand side describes advective transport and $Q(\mathbf{x}_i, \hat{p}_j)$ represents a source term, $i(\mathbf{x}_i, \hat{p})$, integrated over the j_{th} bin. Finally, $b(\hat{p}) \equiv dp/dt$ describes mechanical and radiative loss terms [see Miniati (2001) for further details]. For the energy range of interest here, the most effective among these are synchrotron and inverse Compton emission.

The simulation data allow us to compute various quantities directly related to the observations reported in § 4. Being interested in radio emission, we have computed the synchrotron emission from the simulated relativistic electrons and magnetic field distribution. We have then integrated the emissivity along one of the coordinate axis of the computational box to create a radio map. In general we find that shocks around large, massive structures such as groups and clusters, are relatively bright radio sources. A detailed, quantitative analysis of the properties of radio emission at cosmic shocks is presented in Miniati et al. (2001b).

In order to investigate the physical conditions of the cosmic environment where the CREs are accelerated, we also have obtained analogous maps of inverse Compton hard X-ray (HXR) at 50 keV (from the same relativistic electrons responsible for the radio emission) and of X-ray emission in the 0.5-2 keV band from thermal bremsstrahlung of the collapsed structures.

A portion of size 10 Mpc comoving corresponding to the same structure from each of these maps is presented in Fig. 13. Here we show respectively radio emission in units of '$R_{e/p}^{-1}$ Jy pxl^{-1}' (top left panel), X-ray from thermal bremsstrahlung in units 'erg s^{-1} cm^{-2} pxl^{-1}' (top right), and 50 keV HXR in units '10^{-23} $R_{e/p}^{-1}$ erg s^{-1} cm^{-2} Hz^{-1} pxl^{-1}' (bottom right). In these radio/X-ray units, 1 pxl is about $0.34 \times 0.34\,\mathrm{arcmin}^2$. In the bottom left panel we also show 9 iso-contours of the radio emission, ranging from $10^{-5.8}$ to $10^{-4.6}$ and separated by constant factor of $10^{0.15} = \sqrt{2}$. We point out that the presence of $R_{e/p}$ in our radio and HXR units indicates explicitly the dependence of the computed amount of non-thermal emission on the assumed value for this parameter. In addition, the non-thermal emission in the reported figures depends on an assumed ionic energy injection efficiency of order 10% and a magnetic field average strength of 1μG. Based on a comparison of the numerical and observational results, below we indicate slightly modified values (for these quantities) that are required in order for us to reproduce the observed total radio emission. Given the resolution of the simulation and the putative redshift of the source, the original pixel size in the synthetic image was $0.'34$. Thus to better compare with the observational radio images, the value of the emission in the synthetic images has been averaged over a region corresponding to 3×3 pixels. The choice of this particular portion of the maps has the sole purpose of showing the typical morphological and emission properties of a cosmic, supersonic accretion flow. We briefly discuss similarities between the observed (Fig. 6 & Fig. 9) and simulated radio structures although we *do not* expect matching between the two at any level. We notice that although the contours in the synthetic radio map appear more elongated than in Fig. 6, this is particularly due to the use of much fainter contours in the former image.

One feature of general interest concerns the relative location of the radio emission with respect to the thermal X-ray bright source, that is a group/cluster of galaxies. In our synthetic radio map the brightest (southern) emission region is located in correspondence of an accretion shock and sort of drapes around one side of an X-ray group/cluster. On the northern side of this X-ray structure a fainter extended radio source is also present. Some of the emission there is produced by acceleration regions associated to a smaller collapsing object that happens to be on the same line of sight. Several more smaller and fainter X-ray clumps are also present here. In both cases however, one notes that the radio and thermal X-ray emitting regions do not overlap but are somewhat displaced with respect to each other.

In § 5 we have shown how this pattern is also present in the observational data and becomes visible when a superposition of the radio emission at 320 MHz (or 1.4 GHz) with the ROSAT X-ray map (Fig. 11) is carried out (Fig. 12). It is particularly evident in the southern section of the observational images where the thermal X-ray peak lies shifted to the west from the diffuse regions of radio emission which appears to surround the X-ray region from north, east and south. The stronger X-ray peak to the north as well as the extended filament to the south-east also do not have their exact radio correspondences, although radio peaks are present nearby within 1-5 arcmin. What physical process can produce such an effect ?

This is likely due to the fact that the radio emission possibly traces the peripheral regions of strong accretion shocks generating freshly accelerated relativistic particles. These are the regions at the interface between the externel IGM and ICM. In contrast, the bremsstrahlung X-rays come from interior regions of deep gravitational potential wells in which shock heated and compressed gas is accumulating over cosmological time scales. Note that we can confirm this picture from the synthetic images where we can easily delineate the regions of non-thermal and thermal emissions, and non-thermal emission does correlate spatially with strong shocks.

The maps shown in Fig. 13 were used to compute the total flux from radio-synchrotron and thermal bremsstrahlung emission to be compared with the observational values. Given the radio and X-rays bremsstrahlung fluxes obtained from these plots, and the dependence of the radio flux from the properties of the underlying structure as derived in Miniati et al. (2001b), we have estimated the physical parameters characterizing our numerical model for the CR electrons and the size of the underlying structure required to reproduce the measured radio flux. In addition, using the bottom right panel of Fig. 13, we have also computed the expected HXR flux between 20 and 80 keV. In Table 4 we report each of these quantities and we also summarize the assumptions on shock acceleration efficiency and magnetic field strength before we discuss them below.

Table 4
Simulation Results

$P_{\rm CRE}/P_{\rm ram}$	B (μG)	$S_{\rm sync}$(1.4 GHz) (mJy)	$F_{\rm HXR}$(20-80 keV) (erg s^{-1}cm^{-2})	$F_{\rm XBR}$(0.5-2.0 keV) (erg s^{-1}cm^{-2})
10^{-2}	1.5	20-30	4×10^{-13}	$6{\times}10^{-13}$

The radio flux reported in the previous sections for ZwCl 2341.1+0000 is quite large given the redshift of this source. Nevertheless, according to the simulation results, a radio flux of a few $\times 10$ mJy can be produced by shock accelerated CREs if about 1% of the shock ram pressure is converted into CREs and if the magnetic field is of order of 1-2 μG. This computed flux accounts for the contribution from all the sources that are present in the synthetic image, although it is almost entirely produced by the southern radio filamentary structure. The shock accelerated CREs have typically a flat distribution function, *i.e.,* $f(\hat{p}) \propto \hat{p}^{-q}$, $q \sim 4$, implying a radio spectral index $\alpha \approx -0.5$. However, the total radio flux is produced by the contribution of various CREs distributions that, as they leave the acceleration region and propagate away from it, steepen due to inverse Compton and synchrotron losses. Numerically, it is impossible to spatially resolved these populations. However, it is possible to compute their cumulative distribution function within the numerical cell. This is automatically given by the steady state solution of eq. 10 where the source term describes the shock accelerated CREs and the losses are due to inverse Compton and synchrotron emission. This approximation holds as long as the CREs cooling time is much shorter than the lifetime of shocks (see Miniati (2002) for further details). It is easy to show that for a shock accelerated distribution function $f(\hat{p}) \propto \hat{p}^{-q}$ the steady state solution of eq. 10 is of the form $f(\hat{p}) \propto \hat{p}^{-(q+1)}$, $(q+1) = 5$, which implies a radio spectral index $\alpha = -1$.

This value of α is steeper than found in the observational results, although marginally consistent within a 2 σ margin. Table 2 shows that in most of the regions of the radio source a rather flat spectrum $\alpha \approx -0.5$ is favoured. This value is in accord with what expected for a fresh distribution of CR electrons accelerated at a strong shock in the test particle limit (Drury 1983). However, the spatial region sampled by the telescope beam is larger than distance the CR electrons would propagate before being affected by IC and synchrotron losses. In fact, the cooling time against IC losses of a relativistic electron emitting synchrotron radiation at frequency ν_{GHz} in units GHz is $\tau_{IC} = 10^8 (B_\mu/\nu_{GHz})^{1/2}$ yr, where B_μ is the magnetic field in μG. The distance to which such electrons can be carried by the background flow away from the acceleration region is L$= v_{flow}\tau_{IC} = 100\ (v_{flow}/10^3\,{\rm km\,s^{-1}})\ (B_\mu/\ \nu_{GHz})^{1/2}$ kpc. This distance is shorter than the telescope resolution length which at $z \simeq 0.3$ and for the assumed cosmological model, corresponds to 400 kpc (for 1 arcmin). Therefore, in accord with the above picture, we would expect the

spectral index to be steeper than -0.5.

We can also compare the observed spectral index with the "radio relic" sources found in the peripheral regions of clusters which usually have spectral indices $\alpha \lesssim -1$ and some times as steep as $\alpha \lesssim -3$ (Giovannini, Tordi, & Feretti 1999, Slee et al. 2001). In case of relics a very steep radio spectrum is explained in a scenario in which injection of fresh relativistic electrons in these sources is believed to have ceased for a significant fraction of their lifetime. This picture is different from the conditions expected in the radio filament where ongoing *in situ* acceleration is likely to be taking place. Therefore one would expect a spectral index flatter than the relic sources. It seems possible that the extended very steep spectrum source, detected only at 320 MHz to the N-E of main filament, is in fact a region of relic emission, i.e., a remnant of past activity. In any case, a resolution of the spectral index discrepancy between the observed and simulated values requires additional radio observations possibly over a much wider frequency range than explored here, which would allow the detailed spectral shape to be observed.

The above assumptions on the acceleration efficiency are consistent with a scenario in which about 20-30% of the shock ram pressure is converted into ionic CR pressure and an electrons to ions ratio at relativistic energies, $R_{e/p} \sim 3 - 5 \times 10^{-2}$, in the range allowed for the Galactic CRs (Mueller & Tang 1987, Mueller et al. 1995). With the total number of electrons fixed by this choice of parameters for the acceleration efficiency, the measured flux would imply a magnetic field strength of order of 1μG. This is consistent with values inferred from Faraday rotation measures for clusters of galaxies (Clarke, Kronberg, & Böhringer 2001). However, the magnetic fields at accretion shocks have not been probed yet and they could be weaker than assumed above. In this respect, a detection of or an upper limit on the inverse Compton HXR flux would provide an important constraint on the magnetic field strength. According to our estimate, even with an average magnetic field as strong as 1-2μG the HXR flux should amount to about 4×10^{-13} erg s^{-1}cm^{-2}. Finally, the thermal bremsstrahlung emission produced by the underlying collapsed structure generates a flux of about 6×10^{-13} erg s^{-1}cm^{-2}, corresponding to a ~ 5 keV cluster. At the given redshift $z \sim 0.3$ this would imply a total luminosity of $\sim 10^{44}$ erg s^{-1}. It is of interest to compare these values of thermal bremsstrahlung X-rays with those obtained from ROSAT data as reported in § 5 which are of the same order. We point out that these values are associated with the whole emitting structure which, in the case of Fig. 13, consists of a main collapsed object and two smaller structures. These objects are lined up along a filamentary structure and are likely to merge later on as their evolution progresses.

9 Discussion, Conclusions and Outlook for Future

We have presented here the first strong observational evidence for the existence of large-scale shocks originating in the accretion flows of intergalactic gas, as expected in theory of structure formation. The presence of such shocks is inferred from the diffuse radio emission extending over a physical scale of several Mpc, which intriguingly finds a structural counterpart in a filament of optical galaxies and in a distribution of hot, clustered, thermal X-ray emitting gas. The radio emission appears to be the synchrotron radiation from shock accelerated cosmic-ray electrons and is most likely associated with the intergalactic gas as a whole rather than with individual sources. This scenario is supported by our analytical and numerical calculations which indicate that the above model can easily account for the detected emission with conservative assumptions on the shock acceleration efficiency, and with a magnetic field strength of order of a μG.

The implications of these observations are of great cosmological interest, because they probe two important components of cosmic environment: magnetic fields and cosmic-rays. They indicate that magnetic fields of significant strength are present not only in the ICM but also in the diffuse inter-galactic medium, i.e., in the gas that will be shocked as it accretes onto collapsing structures - the precursors of virialized galaxy clusters. In fact, these magnetic fields are responsible not only for providing the scattering centers for the diffusive shock acceleration mechanism to take place, but also for the synchrotron emission that we observed. No significant magnetic field would be present in the post-shock region of the flow, if it were not already present upstream of the shock. Thus we have shown the first observational evidence for the existence of magnetic fields in a super-cluster scale structure. Since it is all but obvious how magnetic fields are amplified up to such large values in cosmic filaments, these findings pose further challenges to theoretical models. At the same time, although particle acceleration at cosmic shocks is expected on theoretical grounds (Bell 1978, Blandford & Ostriker 1978), theoreticians have been "anxiously" waiting for direct or indirect evidence that it really occurs and at what level it could be linked to the origin of radio relics (*e.g.,* Miniati et al. (2001b), Enßlin et al. (1998)). On the other hand, if diffusive shock acceleration takes place with some efficiency during the non-linear stage of large-scale structure formation, cosmic-ray ions accumulating in the forming structure could become dynamically important with interesting cosmological consequences (Miniati et al. 2001a).

The forming structure reported in this paper could also be a source of high energy γ-ray photons produced through CMBR inverse-Compton by relativistic electrons accelerated at large-scale structure formation shock-waves up to 0.5 TeV (Loeb & Waxman 2000). Loeb & Waxman claim that these electrons

are responsible for the whole γ-ray background flux, although according to Miniati (2002), only a small fraction ($\sim$ 10-20%) of such flux could be accounted for by inverse-Compton emission. In any case, strong γ-emission is expected from accretion flows around clusters [Miniati (2002), Keshet et al. (2002), but see also Totani & Kitayama (2000)].

For this reason, the proto-cluster filament ZwCl 2341.1+0000 is an ideal source to check for γ-ray emission. Its diffuse radio luminosity of ~ 40 mJy can be directly translated into an expected γ-ray flux above energy E_γ of $F_\gamma(> E_\gamma) = 10^{-10}\,\mathrm{photons\ cm^{-2}\ s^{-1}}\,(B/\mu\mathrm{G})^{-2}\,(E_\gamma/100\,\mathrm{MeV})^{-1}$. For comparison - the sensitivities of the EGRET and upcoming GLAST surveys are a few 10^{-8} and 10^{-9} photons $\mathrm{cm^{-2}\,s^{-1}}$ respectively, demonstrating that future γ-ray facilities might become sensitive enough to address these issues.

Thus, the system ZwCl 2341.1+0000 provides an interesting laboratory where issues related to several high energy astrophysical phenomena can be observationally explored. Further spectroscopic redshift mesurements and deep imaging of a wider region, in association of sensitive X-ray and γ-ray observations of this structure will allow to study the energetic processes in the inter galactic medium in much greater detail. We hope that they will be able to reveal further the physical mechanisms that produce the relativistic electron population seen here in the radio-synchrotron emission and will probe the distribution of dark matter relative to the luminous matter and the cosmic-ray particles. The detections of similar objects and signatures of shock waves would help to test our understanding of the intergalactic weather (Quilis, Ibnez, & Saez 1998, Miniati et al. 2000, Burns 1998, Enßlin et al. 2001), which is driven by the power of cosmological structure formation flows.

Acknowledgements

We thank Hans Böhringer for kindly providing us with the ROSAT X-ray images and for his many helpful comments. This research has made use of the NASA/IPAC Extragalactic Database (NED) which is operated by the Jet Propulsion Laboratory, Caltech, under contract with the National Aeronautics and Space Administration. We acknowledge the use of National Radio Astronomy Observatory (NRAO) VLA telescope. The National Radio Astronomy Observatory is a facility of the National Science Foundation operated under cooperative agreement by Associated Universities, Inc.

References

Bagchi, J., Pislar, V. & Lima Neto, G.B., MNRAS, 296, L23 (1998)

Baum, W.A., PASP, 71, 106, (1959)

Bell, A.R., MNRAS, 182, 147 (1978)

Bertin, E., & Arnouts, S., A&A, 117, 393 (1996)

Bertschinger, E, 1985, ApJ Sup. , 58, 39

Bhatnagar, S., Gopal-Krishna, & Wisotzki, L., MNRAS, 299, L25, (1998)

Biermann, L., Z. Naturforsch, 5a, 65 (1950)

Blandford, R.D. & Ostriker, J.P., ApJ Lett. , 221, L29 (1978)

Bond, J.R., Kofman, L. & Pogosyan, D., Nature , 380, 603 (1996)

Burns, J. O., Science, 280, 400 (1998)

Carlberg, R. G., Couchman, H. M. P., & Thomas, P. A., ApJ Lett. , 352, L29 (1990)

J.M.Colberg, S.D.M.White, N.Yoshida, T.MacFarland, A.Jenkins, C.S.Frenk, F.R.Pearce, A.E.Evrard, H.M.P.Couchman, G.Efstathiou, J.Peacock, & P.Thomas, MNRAS, 319, 209 (2000)

Cen, R. & Ostriker, J.P., ApJ, 514, 1 (1999)

Clarke, T. E., Kronberg, P. P., & Böhringer, H., ApJ Lett. , 547, L111 (2001)

Condon, J.J., et al., AJ , 115, 1693 (1998)

Daly, R. A. & Loeb, A., ApJ, 364, 451 (1990)

Deiss, B. M., Reich, W., Lesch, H. & Wielebinski, R., A&A, 321, 55 (1997)

Dickey, J.M, & Lockman, F.J., Ann. Rev. A&A, 28, 215, (1990)

Doroshkevich, A.G., et al., MNRAS, 283, 1281, (1996)

Drury, L. O'C., Rep. Prog. Phys., 46, 973, (1983)

Einasto, M., Tago, E., Jaaniste, J., Einasto, J., Andernach, H., A & A Sup. , 123, 119 (1997)

Ellis, R.A., et al., ApJ, 483, 582, (1997)

Ellison, D. C., Berezhko, E. G., & Baring, M. G. 2000, ApJ, 540, 292

Enßlin, T. A., Biermann, P. L., Klein, U., & Kohle, S., A&A, 332, 395 (1998)

Enßlin, T. A., Simon, P., Biermann, P. L., Klein, U., & Kohle, S., Kronberg P. P., & Mack, K.-H., ApJ Lett. , 549, L39 (2001)

Enßlin, T. A., & Gopal-Krishna, A&A, 366, 26 (2001)

Enßlin, T. A., & Brüggen, M., MNRAS, 331, 1011 (2002)

Feretti, L. & Giovannini, G., Diffuse Cluster Radio Sources (Review). in IAU Symp. 175: Extragalactic Radio Sources, Vol. 175, p. 333 (1996)

Furlanetto, S. R., & Loeb, A., ApJ, 556, 619 (2001)

Giovannini, G., Tordi, M., & Feretti, L., NewA, 4, 141 (1999)

Gladders, M.D., Yee, H.K.C., AJ , 120, 2148 (2000)

Gladders, M.D., Lopez-Cruz, O., Yee, H.K.C., & Kodama, T., ApJ, 501, 571 (1998)

Gnedin, N. Y., Ferrara, A., & Zweibel, E. G., ApJ, 539, 505 (2000)

Gopal-Krishna, Wiita, P.J., ApJ Lett. , 560, L115 (2001)

Guiderdoni, B, & Rocca-Volmerange, B., A & A Sup. , 74, 185, (1988)

Henry, J.P., Gioia, I.M., Mullis, C.R., Clowe, D.I., & Luppino, G.A, AJ , 114, 1293 (1997)

Kang, H. & Jones, T. W., ApJ, 447, 994 (1995)

Kang, H., Ryu, D. & Jones, T.W., ApJ, 456, 422 (1996)

Keshet, U., Waxman, E., Loeb, A., Springel, V., & Hernquist, L., astro-ph/0202318, (2002)

Kim, K. -T., Kronberg, P. P., Giovannini, G., Venturi, T., Nature , 341, 720 (1989)

Kim, K.-T., Kronberg, P. P., Dewdney, P. E., & Landecker, T. L., ApJ, 355, 29 (1990)

Kronberg, P. P., Lesch, H. & Hopp, U., ApJ, 511, 56 (1999)

Kulsrud, R.M., Cen, R., Ostriker, J.P. & Ryu, D., ApJ, 480, 481, (1997)

Lima Neto, G. B., Pislar, V., Bagchi, J., A&A, 368, 440 (2001)

Loeb, A. & Waxman, E., Nature , 405, 156 (2000)

Lubin, L.M., Brunner, R., Metzger, M.R., Postman, M., & Oke, J.B., ApJ Lett. , 531, L5 (2000)

Medina-Tanco, G. & Enßlin, T. A. , Astroparticle Physics, 16, 47 (2001)

Miley, G., Ann. Rev. A & A, 18, 165, (1980)

Miniati, F., Ryu, D., Kang, H., Jones, T. W., Cen, R., & Ostriker, J., ApJ, 542, 608 (2000)

Miniati, F., Comp. Phys. Comm. , 141, 17 (2001)

Miniati, F., Ryu, D., Kang, H., & Jones, T. W., ApJ, 559, 59 (2001a)

Miniati, F., Jones, T. W., Kang, H., & Ryu, D., ApJ, 562, 233 (2001b)

Miniati, F., 2002, MNRAS, submitted (astro-ph/0203014)

Mueller, D., et al., in Int. Cosmic Ray Conference, Vol. 3, Rome, 13 (1995)

Mueller, D. & Tang, K.-K., ApJ, 312, 183 (1987)

Norman, C.A., Melrose, D. B. & Achterberg, A., ApJ, 454, 60 (1995)

Palma C., Bauer F.E., Cotton W.D., et al., AJ, 119, 2068 (2000)

Quilis, V., Ibanez, J. M. A. & Saez, D., ApJ, 502, 518 (1998)

Ryu, D., Ostriker, J. P., Kang, H., & Cen, R., ApJ, 414, 1 (1993)

Ryu, D., & Kang, H., MNRAS, 284, 416 (1997)

Ryu, D., Kang, H., Biermann, P.L., A&A, 335, 19, (1998)

Schlegel, D.J., Finkbeiner, D.P., & Davis, M., ApJ, 500, 525 (1998)

Schoenmakers A.P., de Bruyn A.G., Rottgering H.J.A., & van der Laan H., A&A, 374, 861 (2001)

Slee, O. B., Roy, A. L., Murgia, M., Andernach, H., Ehle, M., AJ , 122, 1172 (2001)

Stanford, S. A., Eisenhardt, P.R., & Dickinson, M., ApJ, 492, 461, (1998)

Strom R.G.& Willis A.G., A&A, 85, 36, (1980)

Totani T., Kitayama T., ApJ, 545, 572 (2000)

Vikhlinin, A., Markevitch, M., & Murray, S. S., ApJ Lett. , 549, L47 (2001)

Voges W., et al., A&A, 349, 389 (1999)

Willson, M. A., MNRAS, 151, 1 (1970)

York, D. G. et al., AJ , 120, 1579 (2000)

Zwicky, F., et al., Catalogue of Galaxies & of Clusters of Galaxies, (Pasadena, California Institute of Technology, 6 vols.) (1961-68)

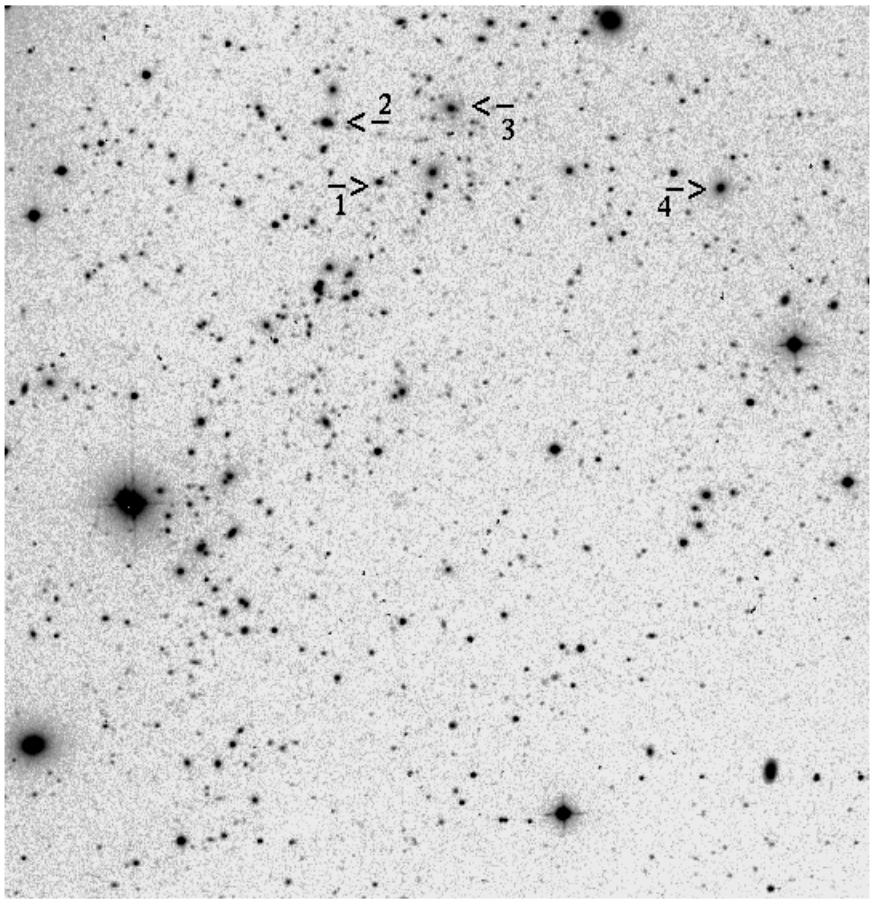

Fig. 1. The co-added R-band CCD image of ZwCl 2341.1+0000. The image shown is an about $12\,'\times\,12\,'$ $(4\times 4\,h_{50}^{-1}\mathrm{Mpc})$ size field with north on top and east to the left. The four galaxies for which the spectroscopic redshifts are available in SDSS and positions are listed in Table 1 are shown by arrows

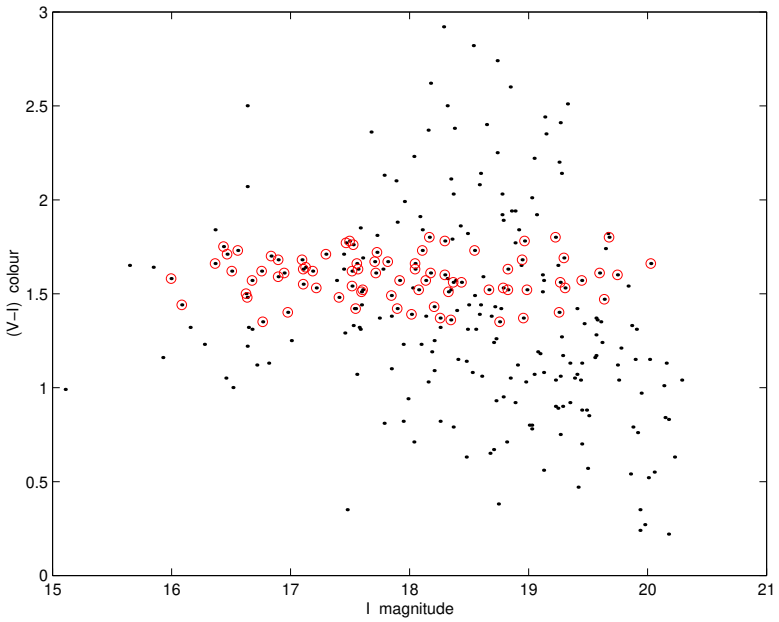

Fig. 2. The $(V-I)$ vs. I colour-magnitude diagram of all detected galaxies in the field of ZwCl 2341.1+0000. The small dots are the data points and encircled dots represent the specific colour selected E/S0 galaxies (see §3.3). Their well defined linear colour-magnitude sequence from the entire field strongly supports the existence of a large-scale structure.

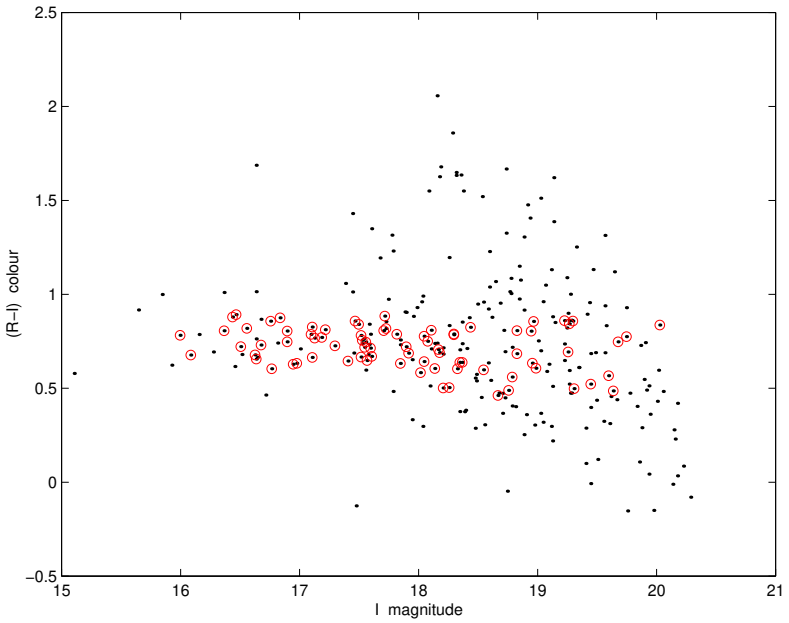

Fig. 3. The $(R-I)$ vs. I colour-magnitude diagram of all detected galaxies in the field of ZwCl 2341.1+0000. The small dots are the data points and encircled dots represent the specific colour selected E/S0 galaxies (see §3.3). Their well defined linear colour-magnitude sequence from the entire field strongly supports the existence of a large-scale structure.

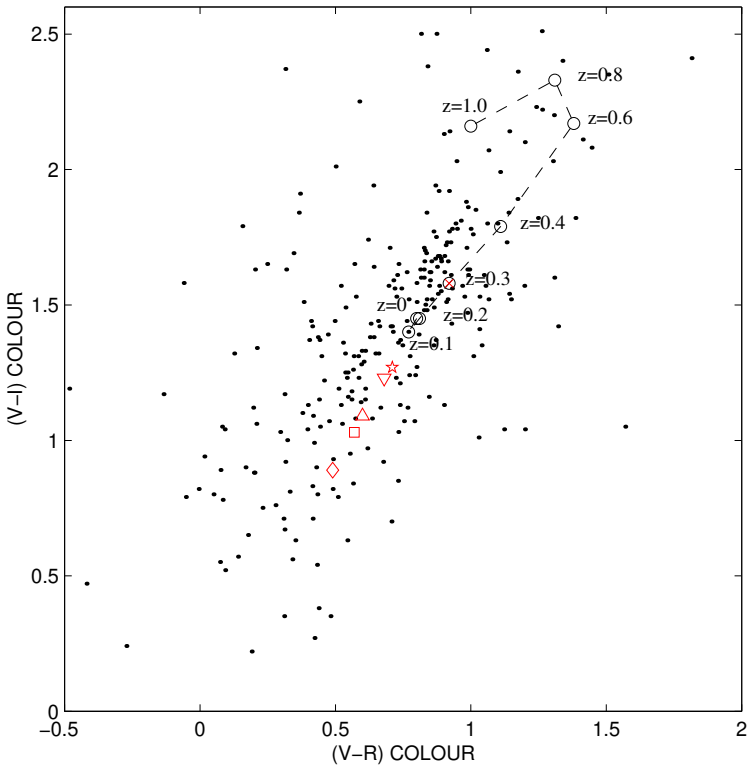

Fig. 4. The $(V-I)$ vs. $(V-R)$ colour-colour diagram of all detected galaxies. The dotted line shows the colour evolutionary track for a model E/S0 galaxy, starting at z=0 and going upto z=1. The redshift values are indicated along the track with open circles. The other symbols represent galaxy colours at z=0.3 of various Hubble types: E/S0 (cross), Sa (star), Sb (downwards triangle), Sc (upwards triangle), Sd (square), Irr (diamond) .

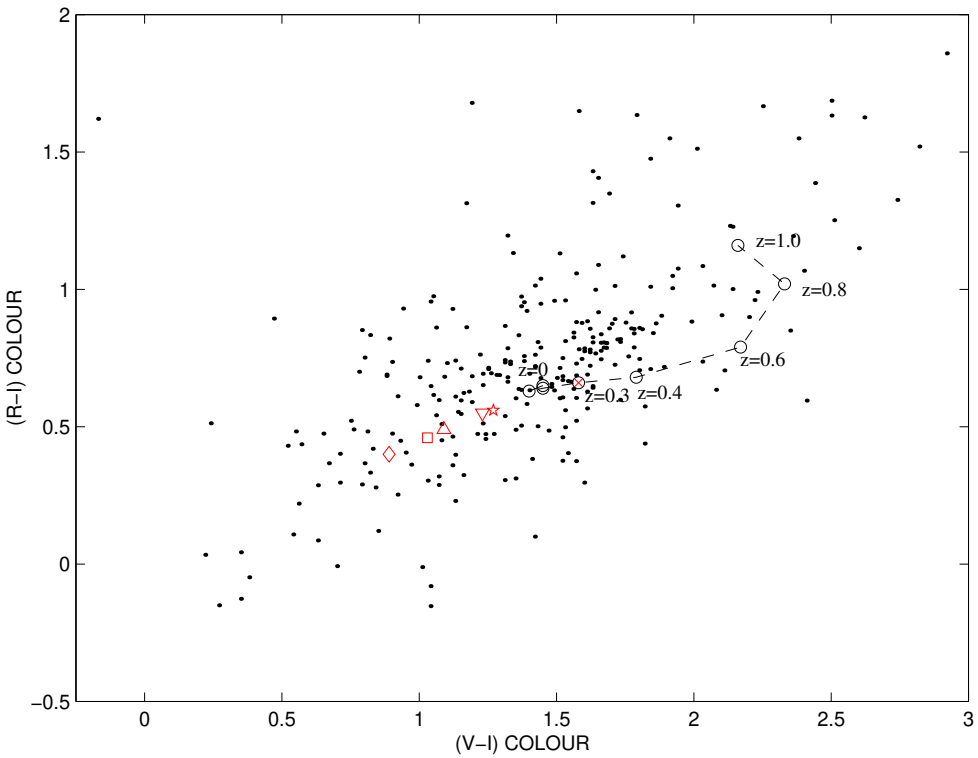
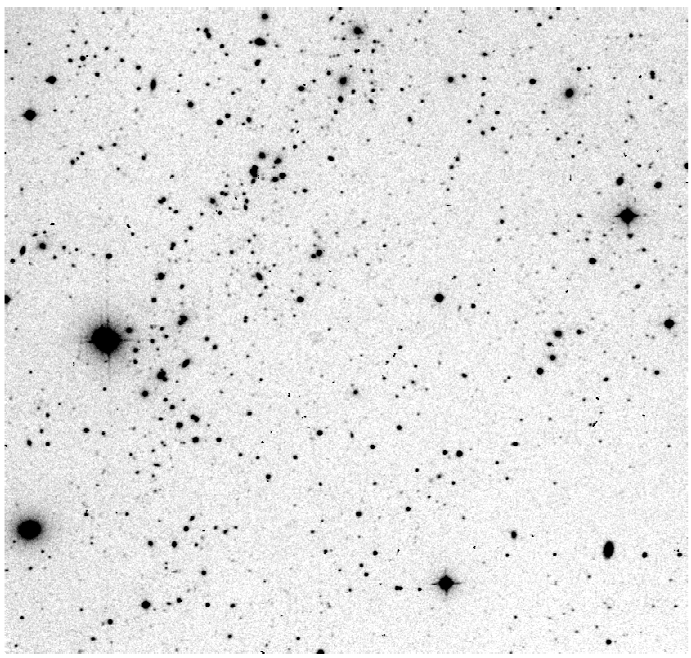
Fig. 5. The $(R-I)$ vs. $(V-I)$ colour-colour diagram of all detected galaxies. The dotted line shows the colour evolutionary track for a model E/S0 galaxy, starting at z=0 and going upto z=1. The redshift values are indicated along the track with open circles. The other symbols represent galaxy colours at z=0.3 of various Hubble types: E/S0 (cross), Sa (star), Sb (downwards triangle), Sc (upwards triangle), Sd (square), Irr (diamond) .